Preprints.org

Article

A Modular Mathematical Model of Fermentation in an Industrial-Scale Bioreactor

Pavel Yu. Kondrakhin [*] , Vladislav A. Kachnov , Ilya R. Akberdin , Fedor A. Kolpakov

Article

A Modular Mathematical Model of Fermentation in an Industrial-Scale Bioreactor

Pavel Yu. Kondrakhin *, Vladislav A. Kachnov, Ilya R. Akberdin and Fedor A. Kolpakov

Department of Computational Biology, Scientific Center for Genetics and Life Sciences, Sirius University of Science and Technology, 354340 Sirius, Russia; vlad.kachnov@gmail.com (V.A.K.); akberdin.ir@talantiuspeh.ru (I.R.A.); kolpakov.fa@talantiuspeh.ru (F.A.K.)

* Correspondence: kondrakhin.py@gmail.com

Abstract: This paper presents a modular hybrid mathematical model of bacterial fermentation developed by integrating a detailed kinetic model for the central carbon metabolism of E. coli with a simplified four-compartment model of a large stirred bioreactor. The model describes the growth dynamics of *E. coli*, taking into account the hydrodynamic characteristics of the cultivation environment and spatial concentration gradients. The first module simulates liquid exchange flows between neighboring reactor zones and tracks the spatial distribution of substrate, acetate, dissolved oxygen, and biomass, while the second one which is a kinetic model includes main metabolic pathways such as glycolysis, the tricarboxylic acid cycle, and oxidative phosphorylation. Numerical simulations reveal how mixing intensity affects concentration gradients and metabolic regimes across the reactor. Additionally, the model was used to identify an optimal mixing regime corresponding to the state where the system first enters the regime of complete aerobic substrate oxidation. The proposed model is applicable for numerical analysis of industrial-scale bioreactors and for predicting metabolic dynamics under various hydrodynamic conditions.

Keywords: bioreactor; mathematical model; modular approach; kinetic model; compartment model; systems biology; BioUML

1. Introduction

The growing challenges of climate change demand effective and sustainable solutions to meet the needs of a rising global population while minimizing environmental impact [1]. Biomanufacturing is the biotechnological production of valuable chemicals [2] which has emerged as a key approach to address these challenges. By relying on renewable alternatives, biomanufacturing helps reduce dependence on fossil-based resources [2–4].

A continuous culturing is widely used in biomanufacturing, as it enables the controlled growth of microorganisms that produce target products. Advances in biological systems engineering have enabled laboratory-scale production of a wide range of compounds, including pharmaceuticals and precursors for materials and fuels, by utilizing microbial chassis at least in small amounts as a proof-of-concept [4–9]. There are also examples of biomanufacturing at an industrial scale, including the production of both high-value products (e.g., therapeutics, enzymes, antibiotics) and low-volume commodities (e.g., bioethanol, lactic acid, amino acids) [10]. However, the successful transition from a laboratory scale (with cultivation volumes ranging from milliliters to tens of liters) [11,12] to an industrial scale (with cultivation volumes reaching hundreds of cubic meters) [13,14] remains challenging and is often associated with significant physical, chemical, and biological limitations [2,12,15]. These constraints often prevent promising developments from being successfully translated into large-scale production [16,17].

One of the key limiting factors during scale-up is the emergence of spatial heterogeneity within large bioreactors. In laboratory-scale bioreactors, rapid mixing (on the order of seconds) results in a

well-mixed, homogeneous environment. In contrast, industrial-scale bioreactors may require several minutes to reach ideal mixing conditions that lead to the formation of zones with concentration gradients of substrate, oxygen, and metabolic products [18,19]. For example, cells may shift toward anaerobic metabolism in zones with limited oxygen availability, leading to the accumulation of acetate – a byproduct that can inhibit microbial growth [20,21]. On the other hand, in substrate-depleted zones, cultures experience nutrient starvation, which reduces overall bioprocess efficiency [21,22].

Mathematical modeling plays a key role in analysis and optimization of industrial bioprocesses, as well as in mitigation of risks during scale-up from laboratory to industrial scale. Four main types of bioreactor models are commonly distinguished: kinetic, compartment, computational fluid dynamics (CFD), and hybrid models. Kinetic models provide a detailed description of metabolic pathways based on chemical kinetics, while generally neglecting hydrodynamic properties of the reactor [23]. In contrast, compartment and CFD models simplify the metabolic representation and instead focus on predicting the formation of mixing gradients. Compartment models consider the reactor as multiple ideally mixed zones (compartments), simulate liquid exchange flows between adjacent zones, and capture concentration gradients of substrate, oxygen, and other key compounds [19,24–26]. CFD models, on the other hand, calculate fluid dynamics by solving the Navier–Stokes equations, treating the liquid phase as a continuous medium [27,28]. While CFD models provide high spatial resolution, they require significant computational resources, making compartment models a computationally inexpensive alternative when moderate detail is sufficient. Finally, hybrid models combine kinetic models with either compartment or CFD models, in order to predict the spatial distribution of compound concentrations under realistic hydrodynamic conditions [29].

The objective of this study was to develop a hybrid mathematical model of an industrial bioreactor that simulates the growth of *E. coli* while accounting for key processes in central carbon metabolism and the spatial environment heterogeneity induced by mixing. To this end, we reproduced results from two previously published models on the BioUML platform: a simplified four-compartment model of a large stirred bioreactor [30] and a detailed kinetic model for the central carbon metabolism of *E. coli* [31]. These models were then combined into a unified modular model.

The structure of the paper is as follows. Section 2 provides a brief overview of the BioUML platform used for the model development and numerical simulations. In Section 3, the modular structure and main equations of the model are detailed. Section 4 presents the simulation results and their interpretation. Section 5 discusses the biological relevance of the results and outlines potential directions for further model refinement. Supplementary Materials (Tables S1–S3) provide the complete description of model equations, parameter values, and initial conditions.

2. Methods

2.1. Modeling Software

Model construction and numerical simulations were carried out using BioUML (Biological Universal Modeling Language, https://sirius-web.org/bioumlweb/), an open-source platform under active development [32,33]. BioUML is a Java-based software environment designed for modeling complex biological systems and analyzing biomedical data. It provides tools for visual representation of modeled biological systems and supports a wide range of systems biology standards, including Systems Biology Markup Language (SBML) [34] and Systems Biology Graphical Notation (SBGN) [35].

Model development in BioUML begins with representation of the modeled system as a compartmentalised graph. Based on this graph, the platform automatically generates Java code that defines the corresponding system of differential equations. Then this code is compiled and executed using internal numerical solvers to simulate the system's dynamics.

To simplify the construction of models for complex systems, BioUML supports a modular approach, which enhances visual clarity and reduces the risk of technical errors. This approach, previously used to build various mathematical models [36,37], allows decomposition of any complex system into elementary components called modules (or submodels/blocks). Each module is defined independently and can follow its own formalism and level of abstraction. Interactions between

modules are defined through variable connections, which, in the context of the bioreactor model, represent processes such as fluid exchange between adjacent compartments.

2.2. Model Parameters

The modular bioreactor model integrates two previously published models, using the same parameter values as reported in the original studies where they were originally described and validated [30,31].

2.3. Numerical Simulations

The unit of model time corresponds to one hour of real time. Numerical simulations were performed using the CVODE solver [38], ported to Java and integrated into the BioUML platform. All simulations presented in this paper were conducted for a duration of up to 1 hour.

3. Modular Model

3.1. Bioreactor Compartmentalization

The bioreactor compartment model utilizes the geometry of a 90-cubic-meter stirred bioreactor with four Rushton turbines, as described in [14,39]. The total reactor volume is divided into four vertical compartments using three horizontal planes, positioned equidistantly between the turbines. Three of the lower compartments have a volume of 20 m³ each, while the top compartment has a volume of 30 m³. A schematic representation of the bioreactor compartmentalization is shown in Figure 1.
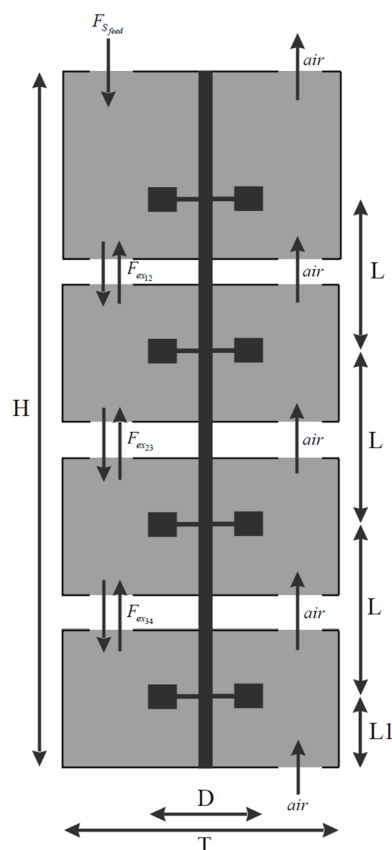

Figure 1. Schematic representation of the bioreactor compartmentalization. Substrate is fed through the top of the reactor ($F_{S_{feed}}$). Bidirectional liquid exchange flows ($F_{ex,i \leftrightarrow j}$) occur between the compartments i and j. Air is supplied to the reactor from the bottom (*air*), with the molar airflow moving only upwards, and no back mixing of the gas phase is considered. Bioreactor geometry: reactor height H=10.464 m, reactor diameter T=3.476 m, distance between turbines L=2.32 m, distance from the bottom turbine to the reactor bottom L1=1.271 m, turbine diameter D=0.936 m.

3.2. Modular Model Structure

The mathematical model of a large stirred bioreactor, which describes the growth of *E. coli* and accounts for key processes in its central carbon metabolism as well as concentration gradients induced by mixing, was developed based on the principles of modular modeling for complex biological systems using the BioUML platform (see Section 2.1).

The BioUML implementation of the model consists of 9 modules: 4 metabolic modules (Metabolic_i) that calculate the dynamics of *E. coli* metabolism in the corresponding reactor zones; 4 compartment modules (Compartment_i) that calculate the liquid exchange flows between neighboring zones; and an auxiliary module (Feed_rate) that calculates the glucose feed rate to the top zone. The modular structure of the model in BioUML is shown in Figure 2.
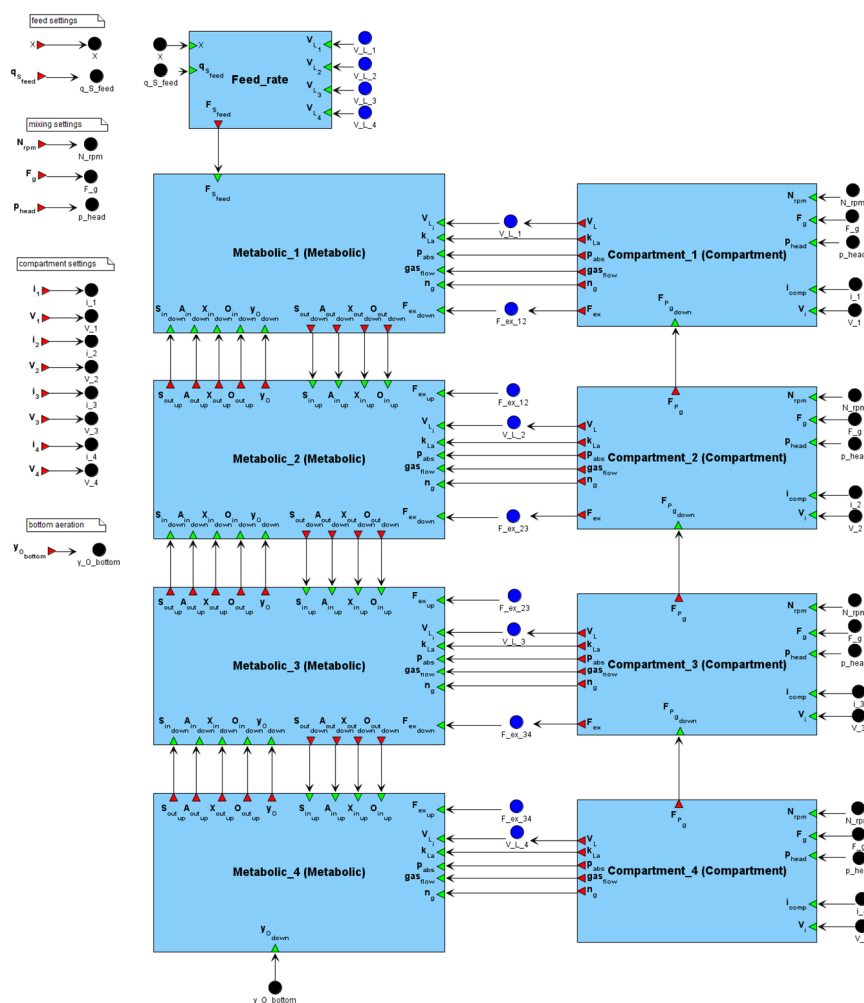
Figure 2. Modular structure of the model. The parameters N_{rpm}, F_g and p_{head} specify the stirrer speed, gas inflow rate, and excess pressure in the top part of the bioreactor, respectively, and together define the mixing intensity. Depending on the mixing regime, the compartment modules calculate the following hydrodynamic quantities: liquid exchange flow F_{ex}, liquid volume in the compartment excluding gas hold-up V_L, oxygen mass transfer coefficient k_{La}, absolute pressure p_{abs}, gas flow rate gas_{flow}, and the number of moles of gas in the compartment n_g. These quantities are transferred to the corresponding metabolic blocks, where they are considered in the calculation of metabolic activity. Neighboring metabolic compartments exchange fluxes of substances, including concentrations of substrate (glucose) S, acetate A, biomass X, dissolved oxygen O, and the mole fraction of oxygen in the gas phase y_O.

The model includes 166 variables, 57 differential equations, 377 parameters, and 96 assignment operations. Hereafter, it is referred to as the modular model of the bioreactor.

3.3. Main Equations of the Modular Model

This section provides a brief overview of the main equations underlying the modular model of the bioreactor (Equations (1) – (23)). A complete description of all equations, parameter values, and initial conditions is given in Supplementary Materials (Tables S1 – S3).

The metabolic modules are based on a previously published kinetic model of the central carbon metabolism of *E. coli* [31]. This model includes the glycolytic pathway, tricarboxylic acid cycle, pentose phosphate pathway, Entner-Doudoroff pathway, anaplerotic pathway, glyoxylate shunt, oxidative phosphorylation, phosphotransferase and non- phosphotransferase systems, and alternative metabolic pathways. Regulation of metabolic activity is also incorporated through four key transcription factors: the cAMP receptor protein, the catabolite repressor/activator, the pyruvate dehydrogenase complex repressor, and the isocitrate lyase regulator.

The dynamics of each metabolic module are governed by the following set of equations (Equations (1) – (4)):

$$\frac{dX}{dt} = \mu\left(\mathbf{x_1}, \mathbf{x_2}, \mathbf{y}, \mathbf{p}\right) X - DX, \tag{1}$$

$$\frac{d\mathbf{y}}{dt} = D\left(\mathbf{y}_{feed} - \mathbf{y}\right) - \mathbf{g}\left(\mathbf{x}_1, \mathbf{x}_2, \mathbf{y}, \mathbf{p}\right) X, \tag{2}$$

$$\frac{d\mathbf{x}_1}{dt} = \mathbf{f}\left(\mathbf{x}_1, \mathbf{x}_2, \mathbf{y}, \mathbf{p}\right), \tag{3}$$

$$\mathbf{x}_2 = \mathbf{h}\left(\mathbf{x}_1, \mathbf{y}, \mathbf{p}\right), \tag{4}$$

where X denotes the biomass concentration in the compartment; $\mathbf{x_1}$ is the vector of time-dependent intracellular variables (e.g., concentrations of metabolites, proteins and enzymes); $\mathbf{x_2}$ is the vector of auxiliary variables, including intracellular regulatory proteins (such as transcription factors and their complexes with metabolites); $\mathbf{y}$ is the vector of extracellular concentrations of glucose and acetate; the vector $\mathbf{y}_{feed}$ contains the concentrations of glucose and acetate in the feeding medium; $\mathbf{p}$ is the vector of the kinetic parameters of the model; and D is the dilution rate. The function $\mu(\mathbf{x_1}, \mathbf{x_2}, \mathbf{y}, \mathbf{p})$ defines the specific growth rate; $\mathbf{g}(\mathbf{x_1}, \mathbf{x_2}, \mathbf{y}, \mathbf{p})$ corresponds to the specific uptake rates of glucose and acetate; and $\mathbf{f}(\mathbf{x_1}, \mathbf{x_2}, \mathbf{y}, \mathbf{p})$ represents the system of intracellular mass balance equations.

To incorporate mixing dynamics, the system was extended with compartment modules based on the simplified compartment model of a bioreactor [31]. The total reactor volume was divided into four compartments (see Section 3.1). To simulate the mixing process, additional exchange terms were introduced into the right-hand side of the differential equations describing the extracellular concentrations of glucose, acetate, and biomass in the metabolic modules (Equations (5) – (7)):

$$S_{i,flow} = \frac{1}{V_{L,i}}\left(\sum F_{ex,j \leftrightarrow i} \cdot S_j - \sum F_{ex,i \leftrightarrow j} \cdot S_i\right), \tag{5}$$

$$A_{i,flow} = \frac{1}{V_{L,i}}\left(\sum F_{ex,j \leftrightarrow i} \cdot A_j - \sum F_{ex,i \leftrightarrow j} \cdot A_i\right), \tag{6}$$

$$X_{i,flow} = \frac{1}{V_{L,i}}\left(\sum F_{ex,j \leftrightarrow i} \cdot X_j - \sum F_{ex,i \leftrightarrow j} \cdot X_i\right), \tag{7}$$

where S, A and X correspond to the extracellular concentrations of glucose, acetate, and biomass, respectively, and $F_{ex,j \leftrightarrow j}$ represents the liquid exchange flow between neighboring compartments *i* and *j*.

The calculation of liquid exchange between compartments was based on the volumetric pumping capacity of Rushton turbines under aerated conditions. It was assumed that half of the liquid flow generated by a turbine is directed downwards and the other half upwards [40,41]. Thus, the liquid exchange flow between compartments *i* and *j* ($F_{ex,j \leftrightarrow j}$) was defined as the average of the two volumetric flows meeting at the interface between these compartments (Equation (8)):

$$F_{ex,i \leftrightarrow j} = \frac{\theta_{P,g,i} + \theta_{P,g,j}}{4}, \tag{8}$$

with the following expressions (Equations (9) – (15)) used to compute intermediate parameters:

$$\theta_{P,g,i} = 0.2 \cdot N_P \cdot \left(\frac{P_g}{P_O}\right)_i \cdot N \cdot D^3, \tag{9}$$

$$\left(\frac{P_g}{P_O}\right)_i = 0.0312 \cdot Fr^{-0.16} \cdot Re^{0.064} \cdot \left(\frac{Q_{g,i}}{N \cdot D^3}\right)^{-0.38} \cdot \left(\frac{T}{D}\right)^{0.8},$$

$$\tag{10}$$

$$Re = \frac{\rho_L \cdot N \cdot D^2}{\eta}, \tag{11}$$

$$Fr = \frac{N^2 \cdot D}{g}, \tag{12}$$

$$Q_{g,i} = \frac{F_g}{\rho_{g,i}}, \tag{13}$$

$$\rho_{g,i} = 10^5 \cdot \frac{p_{abs,i} \cdot MW_G}{R \cdot Temp}, \tag{14}$$

$$p_{abs,i} = \frac{\rho_L \cdot g \cdot h_i}{10^5} + p_{head} + p_{atm}, \tag{15}$$

where $Q_{P,g,i}$ is the volumetric pumping capacity of a single Rushton turbine (with a power number N_P) in compartment i under aeration; P_g/P_O is the ratio of aerated to unaerated power input; Re and Fr are the Reynolds and Froude numbers, respectively; D and N are the impeller diameter and rotation speed; T is the reactor diameter; ρ_L is the liquid density; η is the dynamic viscosity; g is the gravitational acceleration; $Q_{g,i}$ and F_g denote the volumetric and mass flow rates of the gas, respectively; $\rho_{g,i}$ is the gas density; MW_G is the molecular weight of air; $p_{abs,i}$ is the absolute pressure; R is the universal gas constant; $Temp$ is the absolute temperature; h_i is the height of the liquid above the impeller; p_{head} is the excess pressure in the headspace of the reactor; and p_{atm} is the atmospheric pressure.

The original kinetic model of *E. coli* central metabolism [31] did not account for changes in oxygen concentration. Therefore, in the modular model of the bioreactor developed in this study, oxygen dynamics were incorporated by adapting the gas–liquid mass transfer equations from the compartment model of the bioreactor [30].

The gas hold-up (i.e., the volume fraction of the gas relative to the total volume) in each compartment was calculated using the following expressions (Equations (16) – (18)):

$$(1-\varepsilon)_i = 0.13 \cdot \left(\frac{P_{s,i}}{V_i}\right)^{\frac{1}{3}} \cdot \left(v_{g,i}\right)^{\frac{2}{3}}, \tag{16}$$

$$P_{s,i} = N_P \cdot \left(\frac{P_g}{P_O}\right)_i \cdot \rho_L \cdot N^3 \cdot D^5, \tag{17}$$

$$v_{g,i} = \frac{Q_{g,i} \cdot 4}{\pi \cdot T^2}, \tag{18}$$

where ε_i represents the volume fraction of the bulk liquid; V_i is the compartment volume; $P_{g,i}$ is the power input by a single impeller under aeration; and $v_{g,i}$ is the superficial gas velocity. Due to the gas hold-up, the total liquid volume across all compartments is slightly reduced compared to the full bioreactor volume of 90 m³.

Oxygen transfer from the gas phase to the bulk liquid in each compartment was modeled under the assumption that air bubbles do not coalesce. The following expressions (Equations (19) – (21)) were used:

$$OTR_i = (k_L A)_i \cdot \left(O_i^* - O_i\right), \tag{19}$$

$$(k_L A)_i = 0.002 \cdot \left(\frac{P_{g,i}}{V_{L,i}}\right)^{0.7} \cdot v_{g,i}^{\,0.2}, \tag{20}$$

$$O_i^* = y_{O,i} \cdot p_{abs,i}, \tag{21}$$

where OTR_i is the oxygen transfer rate; k_{La} is the oxygen mass transfer coefficient; O_i is the extracellular oxygen concentration; O_i^* is the oxygen saturation concentration; $V_{L,i}$ is the bulk liquid volume; and $y_{O,i}$ is the mole fraction of oxygen in the gas phase.

The following expressions (Equations (22),(23)) were incorporated into the metabolic modules to compute the extracellular oxygen concentration:

$$\frac{dO_i}{dt} = O_{i,flow} + OTR_i, \tag{22}$$

$$\frac{dy_{O,i}}{dt} = \frac{\left(gas_{flow,j \to i} \cdot \left(y_{O,j} - y_{O,i}\right) - OTR_i \cdot V_{L,i}\right)}{n_{g,i}}, \tag{23}$$

where $gas_{flow,j \leftrightarrow i}$ is the gas flow rate and n_g is the number of moles of gas in the compartment.

The resulting extracellular oxygen concentration is consumed by the cells and subsequently utilized in oxidative phosphorylation, with the corresponding reaction rate contributing to the calculation of the specific growth rate. It is worth to note that the original metabolic model considers adaptation to oxygen availability according to an assumption of the oxygen excess in the medium, which allows for the instantaneous recovery of ATP, while the rate of ATP consumption is used in the rate of biomass production (Equations (24) – (28)):

$$\frac{dX}{dt} = \mu X, \tag{24}$$

$$\mu = k_{ATP} v_{ATP}, \tag{25}$$

$$v_{ATP} = OP_{NADH} + OP_{FADH2} - v_{Glk} - v_{Pfk} + v_{Gapdh} + v_{Pyk}$$
$$- v_{Pps} + v_{Ack} - v_{Acs} + v_{\alpha kgdh} - v_{Pck} - v_{AceK} - v_{Cya}, \tag{26}$$

$$OP_{NADH} = \left(v_{Gapdh} + v_{Pdh} + v_{\alpha kgdh} + v_{Mdh}\right) \cdot \left(P/O\right), \tag{27}$$

$$OP_{FADH2} = v_{Sdh}\left(P/O\right)^*, \tag{28}$$

where X is the biomass concentration; μ is the specific growth rate; v_{ATP} is the total ATP production flux; k_{ATP} is the adjustable constant; OP_{NADH} and OP_{FADH2} are the specific ATP production fluxes through oxidative phosphorylation; (P/O) and $(P/O)^*$ indicate the phosphate/oxygen ratios for NADH and FADH2, respectively under aerobic conditions; and v_{Glk}, v_{Pfk}, v_{Gapdh}, v_{Pyk}, v_{Pps}, v_{Ack}, v_{Acs}, $v_{\alpha kgdh}$, v_{Pck}, v_{AceK}, v_{Cya}, v_{Pdh}, v_{Mdh}, v_{Sdh} are reaction rates for glucokinase, phosphofructokinase, glyceraldehyde 3-phosphate dehydrogenase, pyruvate kinase I, phosphoenolpyruvate synthase, acetate kinase, acetyl coenzyme A synthetase, α-keto-D-gluconate dehydrogenase, phosphoenolpyruvate carboxykinase, isocitrate dehydrogenase phosphatase/kinase, adenylate cyclase, pyruvate dehydrogenase, malate dehydrogenase, succinate dehydrogenase, respectively.

While in the proposed model, ATP is restored depending on the accumulated NADH and FADH2 and available oxygen (Equations (29) – (30)):

$$OP_{NADH} = \frac{v_{OP,max} \cdot NADH \cdot O}{\left(K_{OP,NADH} + NADH\right)\left(K_{OP,O} + O\right)} \cdot \left(P/O\right), \tag{29}$$

$$OP_{FADH2} = \frac{v_{OP,max} \cdot FADH2 \cdot O}{\left(K_{OP,FADH2} + FADH2\right)\left(K_{OP,O} + O\right)} \cdot \left(P/O\right)^*, \tag{30}$$

where $NADH$, $FADH2$ and O are concentrations of NADH, FADH2 and intracellular oxygen, respectively; $v_{OP,max}$ is the maximum oxidative phosphorylation rate; $K_{OP,NADH}$ and $K_{OP,FADH2}$ are Michaelis–Menten constants.

Nevertheless, the process of oxidative phosphorylation is presented in a simplified form, taking into account the production of NADH, FADH2 and ATP. The absence of a complete oxidative phosphorylation process can become critical, especially in conditions of changing oxygen concentrations in the compartments of the bioreactor. This constraint is a jumping-off point of further development of the metabolic part of the modular model.

4. Results

4.1. Preliminary Information

The results of the numerical simulations for the modular model of the bioreactor are presented for a total simulation time of 1 hour, which was sufficient for the system to reach a steady state. It should be noted that reaching the stationary growth phase in bacterial cultures typically requires a longer timescale (5–10 hours) [43–47]. This highlights the need for further investigation of the factors and conditions influencing the long-term bioprocess dynamics, which will be addressed in future developments of the presented modular model.

Two different bioreactor mixing regimes were used: one corresponded to low mixing intensity (also referred to as "low settings") with parameter values $N = 80$ rpm, $F_g = 0.4$ kg/s, $p_{head} = 0$ bar; and another corresponded to high mixing intensity ("high settings") with $N = 140$ rpm, $F_g = 0.79$ kg/s, $p_{head} = 1$ bar. Additional simulations were performed by varying the mixing parameters between these two boundaries in order to identify an optimal mixing regime.

In all simulations, the specific glucose feed rate $q_{S_{feed}}$ was set to 0.08 grams of substrate per gram of biomass per hour (gS/gX/h).

### 4.2. Simulation Results for the Boundary Mixing Regimes

Figure 3 shows the dynamics of extracellular metabolite concentrations and biomass across different compartments of the bioreactor under low and high mixing intensities.

At low mixing intensity (Figure 3, left column), oxygen depletion occurs in the upper compartments of the reactor because the upward transport of oxygen from the bottom zones is insufficient to sustain active metabolism. In contrast, under high mixing intensity (Figure 3, right column), the oxygen concentration remains sufficiently high throughout all compartments, thereby preventing acetate accumulation. Since glucose feeding occurs only in the top compartment, substrate depletion is observed in the lower zones. However, under high mixing intensity, glucose distribution becomes slightly more uniform across compartments, and, combined with high oxygen availability, this leads to an accelerated biomass growth rate.

The obtained results qualitatively agree with experimental observations reported in the published data regarding the influence of hydrodynamic conditions on substrate distribution, oxygen availability, and by-product formation in industrial-scale bioreactors [30].

E. coli can simultaneously assimilate substrates through both aerobic and anaerobic pathways. Under oxygen-limited conditions, the proportion of anaerobic metabolism varies, leading to the development of distinct metabolic regimes depending on the ratio between anaerobic and total substrate uptake rates.

Tables 1 and 2 summarize the simulated substrate uptake rates and the corresponding metabolic regimes under different mixing conditions. The classification criteria for metabolic regimes were adopted from the original compartment model [30]: substrate starvation was defined by a total substrate uptake rate below 0.04 gS/gX/h; oxygen limitation was defined when the anaerobic substrate uptake rate exceeded 0.00001 gS/gX/h; in all other cases, substrate limitation was assumed.
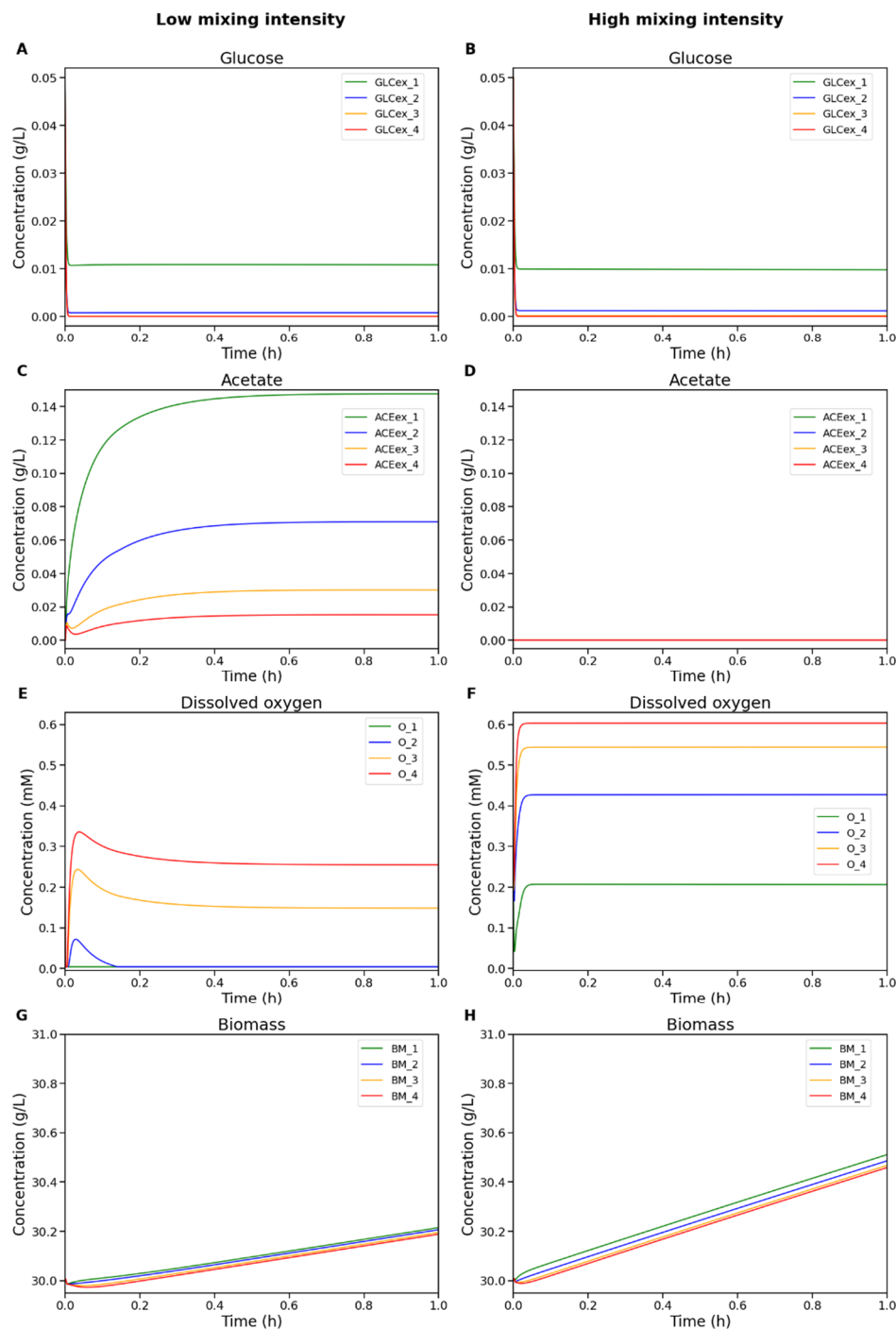
Figure 3. Numerical simulation results of the modular model of the bioreactor under low (left column) and high (right column) mixing intensity. The plots show concentrations of (**A,B**) glucose, (**C,D**) acetate, (**E,F**) dissolved oxygen, and (**G,H**) biomass in the cultivation medium. Colors indicate compartment identity: green – compartment 1 (top), blue – 2, orange – 3, red – 4 (bottom).

Three metabolic regimes were identified from the simulations: oxygen limitation, substrate limitation, and substrate starvation. Under oxygen limitation, the oxygen transfer rate into the liquid phase is insufficient to fully oxidize the available substrate, forcing cells to partially shift to anaerobic metabolism. Substrate starvation occurs when the substrate uptake rate is too low to sustain cell growth, while metabolism remains fully aerobic. In the substrate limitation regime, growth is constrained by the availability of substrate, and all consumed substrate is completely oxidized without switching to anaerobic pathways.

Table 1. Simulated substrate uptake rates and corresponding metabolic regimes in bioreactor compartments under low mixing intensity.

Compartment	Total substrate uptake (gS/gX/h)	Anaerobic substrate uptake (gS/gX/h)	Metabolic regime
1 (top)	0.2245	0.1984	Oxygen limitation
2	0.0196	0.0	Substrate starvation
3	0.0015	0.0	Substrate starvation
4 (bottom)	1.2522×10^{-4}	0.0	Substrate starvation

Table 2. Simulated substrate uptake rates and corresponding metabolic regimes in bioreactor compartments under high mixing intensity.

Compartment	Total substrate uptake (gS/gX/h)	Anaerobic substrate uptake (gS/gX/h)	Metabolic regime
1 (top)	0.2123	0.0	Substrate limitation
2	0.0304	0.0	Substrate starvation
3	0.0038	0.0	Substrate starvation
4 (bottom)	5.4551×10^{-4}	0.0	Substrate starvation

It can be seen that adjusting the mixing parameters primarily influences whether glucose is consumed aerobically or anaerobically in the upper part of the reactor, while the lower compartments still experience significant substrate depletion. Interestingly, increasing the mixing intensity did not reduce the overall extent of substrate starvation across the reactor. This observation is consistent with the well-known fact that Rushton turbines promote efficient radial mixing but do not contribute to better axial (vertical) mixing [19,42]. As a result, glucose remains unevenly distributed along the height of the reactor, and enhanced mixing primarily improves oxygen transfer rather than homogenizing substrate concentrations.

4.3. Optimal Mixing Regime Identification

In addition to the two boundary regimes (with low and high mixing intensity), a series of simulations was conducted by varying three mixing-related parameters within the range defined by their respective boundary values using linear interpolation:

$$par = par_{ls} + \alpha \cdot \left(par_{hs} - par_{ls} \right), \qquad (31)$$

where $par \in \{N, F_g, p_{head}\}$ is the new value of the interpolated parameter; par_{ls} and par_{hs} are its values under low and high mixing settings, respectively; and α is the interpolation coefficient. A value of $\alpha = 0$ corresponds to the low settings, while $\alpha = 1$ corresponds to the high settings.

The aim of this analysis was to determine the minimum value of α at which the steady-state acetate concentration in all compartments stabilizes at zero. This state was interpreted as an optimal mixing regime, in which anaerobic metabolism is fully suppressed at a lower mixing intensity than in the high settings scenario. This regime avoids excessive energy consumption stirring while maintaining optimal conditions for biomass growth.

For each value of $\alpha \in [0,1]$ with a step size of 0.01, a numerical simulation was performed, and the maximum acetate concentration across all compartments was recorded at the final simulation time point. Additionally, it was verified that the system had reached steady state. The resulting

dependency is shown in Figure 4. The dynamics of extracellular metabolite and biomass concentrations for the identified optimal mixing regime are shown in Figure 5.
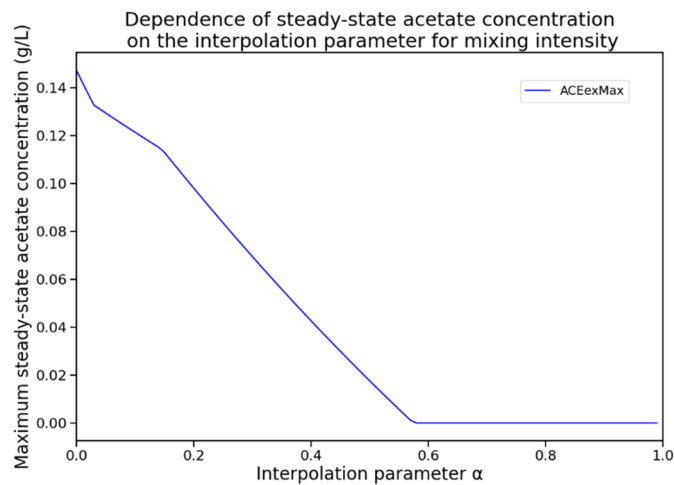
Figure 4. Dependence of the maximum steady-state acetate concentration (ACEexMax) across all compartments on the interpolation parameter α, which defines the mixing intensity.
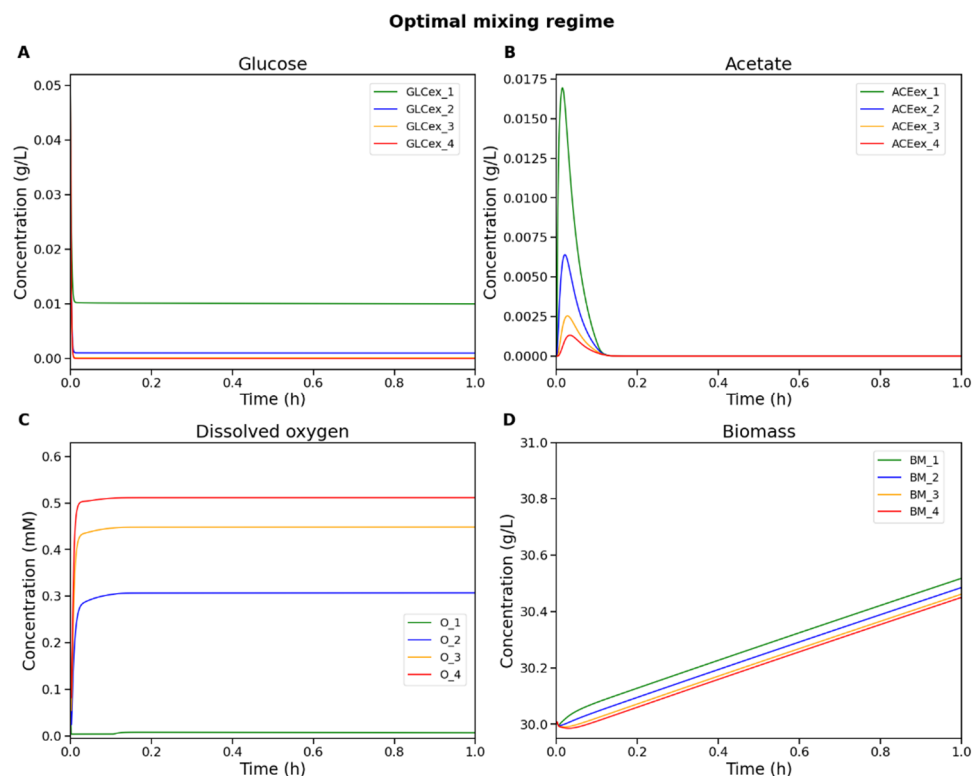
Figure 5. Numerical simulation results of the modular model of the bioreactor under the optimal mixing regime. The plots show concentrations of (**A**) glucose, (**B**) acetate, (**C**) dissolved oxygen, and (**D**) biomass in the cultivation medium. Color coding for compartments is the same as in Figure 3.

The acetate concentration was found to reach zero for the first time at $\alpha \approx 0.58$, which corresponds to a mixing regime with the following parameter values: $N = 114.8$ rpm, $F_g = 0.6262$ kg/s, $p_{head} = 0.58$ bar.

Thus, the simulation results identified a minimum combination of mixing-related parameters at which acetate accumulation was suppressed in all compartments. This transition to fully aerobic substrate oxidation represents an optimal operating regime that sustains biomass growth rates comparable to those under high mixing conditions, while requiring lower energy demands for mixing.

5. Discussion

Fermentation processes in industrial-scale bioreactors are the focus of extensive experimental and computational research [18,48–50]. In this study, we developed a modular mathematical model of an industrial-scale stirred bioreactor capable of simulating the dynamics of metabolic processes in *E. coli* within different bioreactor zones, while explicitly accounting for concentration gradients induced by mixing. The main advantage of the model lies in its integration of a detailed kinetic description of the central carbon metabolism with a simplified hydrodynamic representation of the cultivation environment. This hybrid modeling approach provides an improved capability to capture how mixing conditions and spatial concentration gradients affect the metabolic responses of cell cultures.

The simulation results demonstrated that mixing intensity has a substantial impact on the overall dynamics within the reactor. Under low mixing intensity, oxygen limitation was observed in the upper reactor compartments, forcing cells to partially switch to anaerobic metabolism and leading to acetate accumulation. In contrast, under high mixing intensity, both substrate and oxygen are more evenly distributed, preventing acetate formation and enhancing biomass growth. Additionally, computational analysis allowed identification of an optimal mixing regime, characterized by zero steady-state acetate concentration at more than 40% lower mixing intensity compared to the high-mixing scenario. This result highlights the model's potential in identifying energy-efficient bioreactor operating conditions, which simultaneously improve oxygen availability for aerobic metabolism and reduce risks of mechanical stress on cells associated with excessively high mixing rates [51,52].

However, the current implementation of the modular model relies on a simplified four-compartment representation of hydrodynamics, which does not account for potential intra-compartmental gradients of substrate and oxygen concentrations. This simplification leads to artificially steep transitions between metabolic regimes. In realistic systems, it is reasonable to expect an intermediate region between zones of oxygen limitation and substrate starvation – where substrate is still available but no longer sufficient to meet the full metabolic demands of the cells. The existence of such transitional regions has been computationally confirmed using CFD-based models [30].

Therefore, future improvements of the presented model should focus on incorporating more refined spatial concentration distributions, either by increasing the complexity of compartmentalization or by integrating CFD approaches.

6. Conclusions

In this study, we developed a modular mathematical model of an industrial-scale stirred bioreactor, integrating key aspects of *E. coli* metabolism with hydrodynamic properties of the cultivation environment. The model combines a simplified four-compartment model of a large stirred bioreactor with a detailed kinetic model for the central carbon metabolism of *E. coli*.

The compartment model divides the reactor volume into distinct zones and calculates local concentrations of glucose, oxygen, acetate, and biomass, as well as liquid exchange flows between adjacent compartments. The kinetic model incorporates detailed metabolic pathways, including glycolysis, the tricarboxylic acid cycle, oxidative phosphorylation, and accounts for shifts between aerobic and anaerobic metabolism based on oxygen availability. Compared to existing hybrid models that combine metabolic kinetics with hydrodynamic effects, the presented model provides the most detailed kinetic component, enabling more accurate simulation of metabolic pathways.

Numerical simulation results demonstrated the substantial impact of mixing parameters on spatial distributions of compounds and corresponding metabolic regimes within the bioreactor. Additionally, computational analysis identified an optimal mixing regime that eliminates anaerobic metabolism while reducing energy consumption for stirring. The developed model provides a computational tool for simulating cultivation processes in industrial bioreactors and analyzing metabolic dynamics under various hydrodynamic conditions.

Supplementary Materials: The following supporting information can be downloaded at the website of this paper posted on Preprints.org, Table S1: Model Reactions; Table S2: Model Variables; Table S3: Model Parameters; File S1: Mathematical Model (.omex).

References

1. Calvin, K.; Dasgupta, D.; Krinner, G.; Mukherji, A.; Thorne, P.W.; Trisos, C.; Romero, J.; Aldunce, P.; Barrett, K.; Blanco, G.; et al. *Climate change 2023: Synthesis report. Contribution of Working Groups I, II and III to the Sixth Assessment Report of the Intergovernmental Panel on Climate Change*; Lee, H., Romero, J., Eds.; Intergovernmental Panel on Climate Change (IPCC): Geneva, Switzerland, 2023. https://doi.org/10.59327/ipcc/ar6-9789291691647

2. Cordell, W.T.; Avolio, G.; Takors, R.; Pfleger, B.F. Milligrams to kilograms: Making microbes work at scale. *Trends in Biotechnology* 2023, 41, 1442–1457. https://doi.org/10.1016/j.tibtech.2023.05.002

3. Noorman, H.J.; Heijnen, J.J. Biochemical engineering's grand adventure. *Chemical Engineering Science* 2017, 170, 677–693. https://doi.org/10.1016/j.ces.2016.12.065

4. Straathof, A.J.J.; Wahl, S.A.; Benjamin, K.R.; Takors, R.; Wierckx, N.; Noorman, H.J. Grand research challenges for sustainable industrial biotechnology. *Trends in Biotechnology* 2019, 37, 1042–1050. https://doi.org/10.1016/j.tibtech.2019.04.002

5. Keasling, J.D. Manufacturing molecules through metabolic engineering. *Science* 2010, 330, 1355–1358. https://doi.org/10.1126/science.1193990

6. Stephanopoulos, G. Synthetic biology and metabolic engineering. *ACS Synthetic Biology* 2012, 1, 514–525. https://doi.org/10.1021/sb300094q

7. Casini, A.; Chang, F.-Y.; Eluere, R.; King, A.M.; Young, E.M.; Dudley, Q.M.; Karim, A.; Pratt, K.; Bristol, C.; Forget, A.; et al. A pressure test to make 10 molecules in 90 days: External evaluation of methods to engineer biology. *Journal of the American Chemical Society* 2018, 140, 4302–4316. https://doi.org/10.1021/jacs.7b13292

8. Lee, S.Y.; Kim, H.U.; Chae, T.U.; Cho, J.S.; Kim, J.W.; Shin, J.H.; Kim, D.I.; Ko, Y.-S.; Jang, W.D.; Jang, Y.-S. A comprehensive metabolic map for production of bio-based chemicals. *Nature Catalysis* 2019, 2, 18–33. https://doi.org/10.1038/s41929-018-0212-4

9. Voigt, C.A. Synthetic biology 2020–2030: Six commercially-available products that are changing our world. *Nature Communications* 2020, 11, 6369. https://doi.org/10.1038/s41467-020-20122-2

10. Jullesson, D.; David, F.; Pfleger, B.; Nielsen, J. Impact of synthetic biology and metabolic engineering on industrial production of fine chemicals. *Biotechnology Advances* 2015, 33, 1395–1402. https://doi.org/10.1016/j.biotechadv.2015.02.011

11. Hemmerich, J.; Noack, S.; Wiechert, W.; Oldiges, M. Microbioreactor systems for accelerated bioprocess development. *Biotechnology Journal* 2018, 13, 1700141. https://doi.org/10.1002/biot.201700141

12. Crater, J.S.; Lievense, J.C. Scale-up of industrial microbial processes. *FEMS Microbiology Letters* 2018, 365, fny138. https://doi.org/10.1093/femsle/fny138

13. Noorman, H. An industrial perspective on bioreactor scale-down: What we can learn from combined large-scale bioprocess and model fluid studies. *Biotechnology Journal* 2011, 6, 934–943. https://doi.org/10.1002/biot.201000406

14. Nadal-Rey, G. *Modelling of gradients in industrial aerobic fed-batch fermentation processes*. Ph.D. Thesis, Technical University of Denmark, Denmark, 2020. https://backend.orbit.dtu.dk/ws/portalfiles/portal/244849808/201001_PhDThesis_GiselaNadalRey.pdf

15. Biggs, B.W.; Alper, H.S.; Pfleger, B.F.; Tyo, K.E.J.; Santos, C.N.S.; Ajikumar, P.K.; Stephanopoulos, G. Enabling commercial success of industrial biotechnology. *Science* 2021, 374, 1563–1565. https://doi.org/10.1126/science.abj5040

16. Kampers, L.F.C.; Asin-Garcia, E.; Schaap, P.J.; Wagemakers, A.; Martins dos Santos, V.A.P. From innovation to application: Bridging the valley of death in industrial biotechnology. *Trends in Biotechnology* 2021, 39, 1240–1242. https://doi.org/10.1016/j.tibtech.2021.04.010

17. de Lorenzo, V.; Couto, J. The important versus the exciting: Reining contradictions in contemporary biotechnology. *Microbial Biotechnology* 2018, 12, 32–34. https://doi.org/10.1111/1751-7915.13348

18. Nadal-Rey, G.; McClure, D.D.; Kavanagh, J.M.; Cornelissen, S.; Fletcher, D.F.; Gernaey, K.V. Understanding gradients in industrial bioreactors. *Biotechnology Advances* 2021, 46, 107660. https://doi.org/10.1016/j.biotechadv.2020.107660

19. Vrábel, P.; van der Lans, R.G.J.M.; Luyben, K.Ch.A.M.; Boon, L.; Nienow, A.W. Mixing in large-scale vessels stirred with multiple radial or radial and axial up-pumping impellers: Modelling and measurements. *Chemical Engineering Science* 2000, 55, 5881–5896. https://doi.org/10.1016/s0009-2509(00)00175-5

20. Xu, B.; Jahic, M.; Enfors, S.-O. Modeling of overflow metabolism in batch and fed-batch cultures of *Escherichia coli*. *Biotechnology Progress* 1999, 15, 81–90. https://doi.org/10.1021/bp9801087

21. Wolfe, A.J. The acetate switch. *Microbiology and Molecular Biology Reviews* 2005, 69, 12–50. https://doi.org/10.1128/mmbr.69.1.12-50.2005

22. Neubauer, P.; Åhman, M.; Törnkvist, M.; Larsson, G.; Enfors, S.-O. Response of guanosine tetraphosphate to glucose fluctuations in fed-batch cultivations of *Escherichia coli*. *Journal of Biotechnology* 1995, 43, 195–204. https://doi.org/10.1016/0168-1656(95)00130-1

23. Almquist, J.; Cvijovic, M.; Hatzimanikatis, V.; Nielsen, J.; Jirstrand, M. Kinetic models in industrial biotechnology – Improving cell factory performance. *Metabolic Engineering* 2014, 24, 38–60. https://doi.org/10.1016/j.ymben.2014.03.007

24. Vrábel, P.; van der Lans, R.G.J.M.; Cui, Y.Q.; Luyben, K.Ch.A.M. Compartment model approach. *Chemical Engineering Research and Design* 1999, 77, 291–302. https://doi.org/10.1205/026387699526223

25. Oosterhuis, N.M.G.; Kossen, N.W.F. Dissolved oxygen concentration profiles in a production-scale bioreactor. *Biotechnology and Bioengineering* 1984, 26, 546–550. https://doi.org/10.1002/bit.260260522

26. Reuss, M.; Bajpai, R. Stirred tank models. In *Biotechnology*; Wiley: 1991; pp. 299–348. https://doi.org/10.1002/9783527620852.ch10

27. Spann, R.; Glibstrup, J.; Pellicer-Alborch, K.; Junne, S.; Neubauer, P.; Roca, C.; Kold, D.; Lantz, A.E.; Sin, G.; Gernaey, K.V.; Krühne, U. CFD predicted pH gradients in lactic acid bacteria cultivations. *Biotechnology and Bioengineering* 2018, 116, 769–780. https://doi.org/10.1002/bit.26868

28. Kuschel, M.; Takors, R. Simulated oxygen and glucose gradients as a prerequisite for predicting industrial scale performance *a priori*. *Biotechnology and Bioengineering* 2020, 117, 2760–2770. https://doi.org/10.1002/bit.27457

29. Spann, R.; Gernaey, K.V.; Sin, G. A compartment model for risk-based monitoring of lactic acid bacteria cultivations. *Biochemical Engineering Journal* 2019, 151, 107293. https://doi.org/10.1016/j.bej.2019.107293

30. Bafna-Rührer, J. *Strategies and tools to select E. coli fermenterphiles for industrial application*. Ph.D. Thesis, Technical University of Denmark, Denmark, 2024. https://orbit.dtu.dk/files/375573898/Submission_version_PhD_thesis_JBR.pdf

31. Jahan, N.; Maeda, K.; Matsuoka, Y.; Sugimoto, Y.; Kurata, H. Development of an accurate kinetic model for the central carbon metabolism of *Escherichia coli*. *Microbial Cell Factories* 2016, 15, 112. https://doi.org/10.1186/s12934-016-0511-x

32. Kolpakov, F.; Akberdin, I.; Kashapov, T.; Kiselev, I.; Kolmykov, S.; Kondrakhin, Y.; Kutumova, E.; Mandrik, N.; Pintus, S.; Ryabova, A.; et al. BioUML: An integrated environment for systems biology and collaborative analysis of biomedical data. *Nucleic Acids Research* 2019, 47, W225–W233. https://doi.org/10.1093/nar/gkz440

33. Kolpakov, F.; Akberdin, I.; Kiselev, I.; Kolmykov, S.; Kondrakhin, Y.; Kulyashov, M.; Kutumova, E.; Pintus, S.; Ryabova, A.; Sharipov, R.; et al. BioUML—towards a universal research platform. *Nucleic Acids Research* 2022, 50, W124–W131. https://doi.org/10.1093/nar/gkac286

34. Hucka, M.; Bergmann, F.T.; Chaouiya, C.; Dräger, A.; Hoops, S.; Keating, S.M.; König, M.; Novère, N.L.; Myers, C.J.; Olivier, B.G.; et al. The Systems Biology Markup Language (SBML): Language specification for Level 3 Version 2 Core Release 2. *Journal of Integrative Bioinformatics* 2019, 16, jib-2019-0021. https://doi.org/10.1515/jib-2019-0021

35. Novère, N.L.; Hucka, M.; Mi, H.; Moodie, S.; Schreiber, F.; Sorokin, A.; Demir, E.; Wegner, K.; Aladjem, M.I.; Wimalaratne, S.M.; et al. The Systems Biology Graphical Notation. *Nature Biotechnology* 2009, 27, 735–741. https://doi.org/10.1038/nbt.1558

36. Kutumova, E.O.; Akberdin, I.R.; Egorova, V.S.; Kolesova, E.P.; Parodi, A.; Pokrovsky, V.S.; Zamyatnin, A.A. Jr; Kolpakov, F.A. Physiologically based pharmacokinetic model for predicting the biodistribution of albumin nanoparticles after induction and recovery from acute lung injury. *Heliyon* 2024, 10, e30962. https://doi.org/10.1016/j.heliyon.2024.e30962

37. Miroshnichenko, M.I.; Kolpakov, F.A.; Akberdin, I.R. A modular mathematical model of the immune response for investigating the pathogenesis of infectious diseases. *Viruses* 2025, 17, 589. https://doi.org/10.3390/v17050589

38. Hindmarsh, A.C.; Brown, P.N.; Grant, K.E.; Lee, S.L.; Serban, R.; Shumaker, D.E.; Woodward, C.S. SUNDIALS. *ACM Transactions on Mathematical Software* 2005, 31, 363–396. https://doi.org/10.1145/1089014.1089020

39. Nadal-Rey, G.; McClure, D.D.; Kavanagh, J.M.; Cassells, B.; Cornelissen, S.; Fletcher, D.F.; Gernaey, K.V. Development of dynamic compartment models for industrial aerobic fed-batch fermentation processes. *Chemical Engineering Journal* 2021, 420, 130402. https://doi.org/10.1016/j.cej.2021.130402

40. Oosterhuis, N.M.G. *Scale-up of bioreactors: A scale-down approach*. Ph.D. Thesis, TU Delft, Netherlands, 1984. http://resolver.tudelft.nl/uuid:03a887b7-8c20-4052-8d6b-7fe76918d7ec

41. Noorman, H.J.; van Winden, W.; Heijnen, J.J.; van der Lans, R.G.J.M. Intensified fermentation processes and equipment. In *Intensification of Biobased Processes*; The Royal Society of Chemistry: 2018; pp. 1–41. https://doi.org/10.1039/9781788010320-00001

42. Lapin, A.; Müller, D.; Reuss, M. Dynamic behavior of microbial populations in stirred bioreactors simulated with Euler–Lagrange methods: Traveling along the lifelines of single cells. *Industrial & Engineering Chemistry Research* 2004, 43, 4647–4656. https://doi.org/10.1021/ie030786k

43. Hewitt, C.J.; Boon, L.A.; McFarlane, C.M.; Nienow, A.W. The use of flow cytometry to study the impact of fluid mechanical stress on *Escherichia coli* W3110 during continuous cultivation in an agitated bioreactor. *Biotechnology and Bioengineering* 1998, 59, 612–620. https://doi.org/10.1002/(sici)1097-0290(19980905)59:5<612::aid-bit12>3.0.co;2-b

44. Guardia Alba, M.J.; García Calvo, E. Characterization of bioreaction processes: Aerobic *Escherichia coli* cultures. *Journal of Biotechnology* 2000, 84, 107–118. https://doi.org/10.1016/s0168-1656(00)00343-6

45. Lapin, A.; Schmid, J.; Reuss, M. Modeling the dynamics of *E. coli* populations in the three-dimensional turbulent field of a stirred-tank bioreactor—A structured–segregated approach. *Chemical Engineering Science* 2006, 61, 4783–4797. https://doi.org/10.1016/j.ces.2006.03.003

46. Glazyrina, J.; Materne, E.-M.; Dreher, T.; Storm, D.; Junne, S.; Adams, T.; Greller, G.; Neubauer, P. High cell density cultivation and recombinant protein production with *Escherichia coli* in a rocking-motion-type bioreactor. *Microbial Cell Factories* 2010, 9, 42. https://doi.org/10.1186/1475-2859-9-42

47. Zambrano, J.; Carlsson, B.; Diehl, S. Optimal steady-state design of zone volumes of bioreactors with Monod growth kinetics. *Biochemical Engineering Journal* 2015, 100, 59–66. https://doi.org/10.1016/j.bej.2015.04.002

48. Garcia-Ochoa, F.; Gomez, E. Bioreactor scale-up and oxygen transfer rate in microbial processes: An overview. *Biotechnology Advances* 2009, 27, 153–176. https://doi.org/10.1016/j.biotechadv.2008.10.006

49.   Tarlak, F. The use of predictive microbiology for the prediction of the shelf life of food products. *Foods* 2023, 12, 4461. https://doi.org/10.3390/foods12244461

50.   de Mello, A.F.M.; de Souza Vandenberghe, L.P.; Herrmann, L.W.; Letti, L.A.J.; Burgos, W.J.M.; Scapini, T.; Manzoki, M.C.; de Oliveira, P.Z.; Soccol, C.R. Strategies and engineering aspects on the scale-up of bioreactors for different bioprocesses. *Systems Microbiology and Biomanufacturing* 2023, 4, 365–385. https://doi.org/10.1007/s43393-023-00205-z

51.   de Lamotte, A.; Delafosse, A.; Calvo, S.; Delvigne, F.; Toye, D. Investigating the effects of hydrodynamics and mixing on mass transfer through the free-surface in stirred tank bioreactors. *Chemical Engineering Science* 2017, 172, 125–142. https://doi.org/10.1016/j.ces.2017.06.028

52.   Garcia-Ochoa, F.; Gomez, E.; Santos, V.E. Fluid dynamic conditions and oxygen availability effects on microbial cultures in STBR: An overview. *Biochemical Engineering Journal* 2020, 164, 107803. https://doi.org/10.1016/j.bej.2020.107803